



Ultrafast reversal of the ferroelectric polarization by a midinfrared pulse

Veniamin A. Abalmasov *

Institute of Automation and Electrometry SB RAS, 630090 Novosibirsk, Russia

 (Received 4 October 2019; revised manuscript received 16 December 2019; published 9 January 2020)

I calculate the ferroelectric polarization dynamics induced by a femtosecond midinfrared pulse as measured in the recent experiment by R. Mankowsky *et al.*, *Phys. Rev. Lett.* **118**, 197601 (2017). It is due to the nonlinear coupling of the excited infrared-active phonon mode with the ferroelectric mode or to the excitation of the ferroelectric mode itself depending on the pulse frequency. To begin with, I write the LiNbO_3 crystal symmetry invariant thermodynamic potential including electric field and nonlinear phonon coupling terms. I solve the equations of motion determined by this potential for phonon coordinates numerically. I explain the transient polarization reversal observed in the experiment by the action of the depolarizing electric field, which is due to bound charges at the polarization domain boundaries, and give a reasonable estimate for its value. I argue that the polarization can be reversed when this field is screened.

DOI: [10.1103/PhysRevB.101.014102](https://doi.org/10.1103/PhysRevB.101.014102)

I. INTRODUCTION

Polarization control is essential for many applications of ferroelectrics, from nonvolatile memory storing [1] to switchable surface chemistry and catalysis [2,3] (see generally [4,5]). The usual mechanism via static or pulsed electric fields leads to the polarization reversal duration limited from below to hundreds of picoseconds [6]. Several proposals have been made how to switch the polarization on the picoseconds time scale by directly exciting the ferroelectric mode with ultrashort radiation pulses [7–9] or the electronic subsystem with optical pulses [10]. However, they still have not been realized in practice, and the excitation by optical pulses has only led to a decrease in polarization [11–13]. Nevertheless, a 90° polarization rotation in some domains of a multi-domain ferroelectric thin film of $(\text{Ba}_{0.8}\text{Sr}_{0.2})\text{TiO}_3$ induced by a strong single-cycle terahertz pulse was claimed recently in [14,15]. At the same time, ultra-short (less than 20 ps) all-optical magnetic polarization control with low heat load in transparent ferromagnetic films has already been reported [16].

Recently, it has been proposed to switch the ferroelectric polarization by resonantly exciting the infrared-active phonon mode nonlinearly coupled to the ferroelectric mode [17]. This approach, called nonlinear phononics and having been developed over several past decades with the advent of very high intensity lasers, has already proved to be successful in ultrafast lattice control [18]. The follow-up experiment [19] has indeed demonstrated a transient switching of the polarization in LiNbO_3 (LNO) crystal for laser pulse fluences larger than about 60 mJ/cm^2 (with the laser pulse duration of about 0.15 ps). One possible explanation of the observed rapid polarization return to its initial state was the formation of uncompensated electric charges in the irradiated part of the crystal after the polarization reversal [19], which has not been taken into account theoretically [7–9,17,19].

Here, I calculate the phonon mode dynamics under conditions similar to those in the experiment [19]. First, I argue that the equation of motion for the polarization is governed by the thermodynamic potential rather than potential obtained from *ab initio* calculations for the unrelaxed crystal which was used in Refs. [17,19]. This implies that the nonlinear coupling terms must be invariant under the symmetry transformations of the crystal parent group. I find the biquadratic coupling constant values from the infrared phonon frequency change at the ferroelectric phase transition, which is known for LNO from *ab initio* calculations only [20–22]. I solve numerically the equations of motion for the coupled phonon modes and determine the depolarizing electric field value that corresponds better to the polarization dynamics observed in Ref. [19]. I propose to screen this field in experiment by a metallic wire deposited on the crystal surface around the irradiated spot in order to get a final polarization reversal. I also show that the polarization reversal is possible under experimental conditions of Ref. [19] when the ferroelectric mode is excited resonantly, though it demands very high pump fluences.

II. THEORETICAL APPROACH

In crystals, the movement of interacting with each other atoms near their equilibrium positions is a superposition of a complete set of normal modes $\{Q\}$. Such modes are plain waves with definite frequencies and polarizations and transform according to irreducible representations of the crystal symmetry group. According to the phenomenological Landau theory, the second order phase transition takes place when the coefficient of the quadratic term of one of the coordinates in the thermodynamic potential $F(\{Q\}, T)$ becomes negative below the critical temperature T_c . This leads to a nonzero thermal equilibrium value of this coordinate, which determines the spontaneous polarization in ferroelectrics [23].

The thermodynamic potential determines as well the dynamics of the order parameter [24]. In the case of a displacive

* abalmasov@iae.nsc.ru

structural phase transition the corresponding equation is

$$\ddot{Q} + \gamma \dot{Q} + \partial F(\{Q\}, T)/\partial Q = 0, \quad (1)$$

where γ is the damping constant. In the static case, this equation reduces to the usual thermal equilibrium condition. For low-frequency coordinates, $F(\{Q\}, T)$ is to be calculated with fixed generalized forces conjugate to all other generalized coordinates. For high-frequency coordinates it should be calculated with fixed values of slowly changing coordinates instead [24]. Thus understood Eq. (1) expresses the essence of the so-called soft mode concept. Indeed, the square frequency in Eq. (1) is equal to the inverse static susceptibility $\chi^{-1}(T) = \partial^2 F(\{Q\}, T)/\partial Q^2$ that becomes zero at $T = T_c$.

The coordinate Q in Eq. (1) can be replaced by the quantum mechanical operator $\hat{Q}(t)$ and the equation remains valid when averaged over the quantum state. This follows from the expression for the time derivative of the expectation of any quantum mechanical operator [25] and is the essence of the Ehrenfest theorem [26]. It should be remembered, however, that when the last term in Eq. (1) is nonlinear in Q , its expectation value, $\langle F(Q) \rangle$, is not equal to $F(\langle Q \rangle)$. For example, the expectation value of the coordinate square, $\langle Q^2 \rangle = \langle Q \rangle^2 + \langle \delta Q^2 \rangle$, is the sum of the square of its expectation value and the quantum fluctuation $\langle \delta Q^2 \rangle = \langle (Q - \langle Q \rangle)^2 \rangle$. Thus, neglect of quantum fluctuations can be justified if $\langle Q \rangle \gg \sqrt{\langle \delta Q^2 \rangle}$. The same applies to the thermal averaging of Eq. (1) and neglect of thermal fluctuations. In the following, I consider the average coordinates and evaluate their fluctuations when discussing the results.

I note that when the damping in Eq. (1) is large, the equation actually describes the relaxation mode and corresponds to the dynamics of the order parameter for the order-disorder phase transition. This occurs in the vicinity of the displacive phase transition when the frequency of the ferroelectric soft mode tends to zero [27].

The potential $V(Q_P, Q_{IR})$, which determines equations of motion similar to Eq. (1), was calculated in Ref. [17] as a function of the ferroelectric and infrared mode coordinates, Q_P and Q_{IR} , for PbTiO_3 crystal from the first principles using the density functional theory. At each point of calculations, the values of all the rest of phonon coordinates were fixed and corresponded to the low-temperature ferroelectric phase. As a result, the potential $V(Q_P)$ was not symmetric in the ferroelectric mode coordinate Q_P even for $Q_{IR} = 0$ (though the symmetry was restored when the other coordinates were relaxed for a given value of Q_P) [17]. The thus obtained potential would be appropriate for a very fast dynamics of the ferroelectric mode when the other coordinates are too slow to relax at each value of Q_P and can be considered as fixed. At the same time, the characteristic time change of Q_P in the experiment [19] is not smaller than its inverse frequency and this coordinate is the slowest. Thus, as discussed above, in order to calculate the thermodynamic potential $F(Q_P, Q_{IR})$, governing the ferroelectric mode dynamics, one should relax the crystal at each value of Q_P . Indeed, the signal of the second harmonics vanishes at some point in Ref. [19]. This implies that the crystal becomes centrosymmetric at that moment that would not be possible when only the polarization vanishes

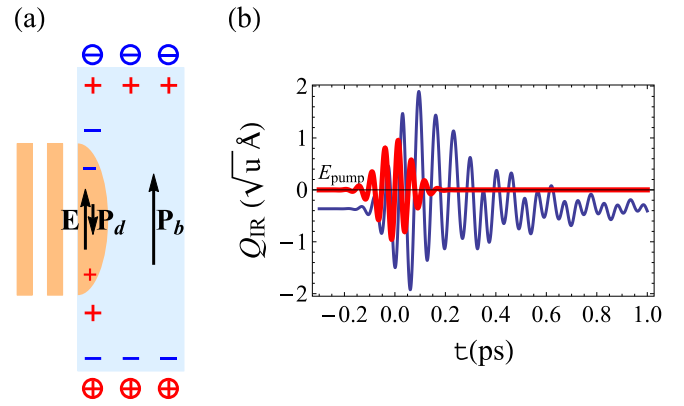


FIG. 1. Sketch of the bulk and domain polarization $\mathbf{P}_{b,d}$ and the electric field \mathbf{E} due to the bound charges in the sample when irradiated by a terahertz pulse; free charges on the surface are drawn with circles (a). Time dependence of the terahertz radiation electric field (thick, red) and the corresponding infrared mode amplitude $Q_{A_1(\text{TO})_4}$ (blue) nonlinearly coupled to the ferroelectric mode at a fluence of 95 mJ/cm^2 (b).

but the values of the other coordinates correspond to the noncentrosymmetric ferroelectric phase as in Ref. [17].

III. LNO THERMODYNAMIC POTENTIAL

In what follows, I will consider the LNO crystal along with the experimental setup and conditions of [19], see Fig. 1. The ferroelectric phase transition in the LNO crystal occurs at a temperature of about 1480 K from the paraelectric phase with symmetry $R3c$ (D_{3d}^6) to the low-temperature ferroelectric phase with symmetry $R3c$ (C_{3v}^6) [20]. Two formula units in the unit cell implies 27 optical phonon modes, $4A_1 + 5A_2 + 9E$ in the ferroelectric phase and $A_{1g} + 2A_{1u} + 3A_{2g} + 3A_{2u} + 4E_g + 5E_u$ in the paraelectric phase. In the ferroelectric phase, the infrared-active phonon modes $A_1(\text{TO}_{1-4})$ have frequencies of about 7.5, 8.1, 10, and 19 THz and the modes $E(\text{TO}_{1-9})$ have frequencies of about 4.6, 7.0, 7.9, 9.7, 10.8, 11.1, 13.0, 17.3, and 19.8 THz [28–30]. The mode $A_1(\text{TO}_3)$ of the ferroelectric phase changes to the A_{1g} in the paraelectric phase while the other modes A_1 become A_{2u} [20]. The $A_1(\text{TO}_1)$ mode becomes softer approaching the phase transition [31] and according to the first-principles calculations [21] it has the strongest overlap (0.82) with the A_{2u} mode, which is unstable in the paraelectric phase and coincides with the atomic displacements during the phase transition. The mixing of the $A_1(\text{TO}_1)$ and $A_1(\text{TO}_2)$ modes at temperatures between 400 and 600 K [31] is probably the cause of the incomplete overlap of the $A_1(\text{TO}_1)$ and A_{2u} modes, mentioned above. I will label the ferroelectric soft mode as Q_P and the other infrared-active modes Q_{IR} as $Q_{A_{1g}}$, $Q_{A_{2u}}$, $(Q_{E_g,x}, Q_{E_g,y})$, and $(Q_{E_u,x}, Q_{E_u,y})$ according to their irreducible representations.

During the ferroelectric phase transition the condensation of the soft mode occurs at the center of the Brillouin zone. The terahertz pulse as in the experiment [19] also excites mostly long-wavelength phonons. So I will consider an homogeneous case and neglect the interaction of phonons with different wavelengths coming from the nonlinear phonon coupling.

The thermodynamic potential density $F(\{Q\}, T)$ should be invariant under transformations of the crystal symmetry group of the parent paraelectric phase. I will write it as a sum

$$F = F_0 + F_{E\text{-ph}} + F_{\text{ph-ph}}. \quad (2)$$

The first part describes free phonons:

$$F_0 = -\frac{\omega_P^2}{4} Q_P^2 + \frac{c_P}{4} Q_P^4 + \frac{\omega_{\text{IR}}^2}{2} Q_{\text{IR}}^2, \quad (3)$$

where $\omega_{P,\text{IR}}$ are frequencies of the corresponding modes $Q_{P,\text{IR}}$. The coefficient c_P determines the equilibrium value Q_P^e through the equation $\partial F/\partial Q_P = 0$. In the absence of electric field and nonlinear phonon interactions this gives $c_P = \omega_P^2/2(Q_P^e)^2$. Summation over all infrared-active modes Q_{IR} in Eq. (3) is assumed.

$F_0(Q_P)$ as a function of the ferroelectric mode amplitude was calculated *ab initio*, for instance, in Ref. [32]. When fitted to a fourth order polynomial, it provided the energy difference between the ground and the lowest excited state of about 7.5 THz in frequency units, in agreement with the experimental data [28–30].

The second part of the thermodynamic potential corresponds to the phonon-electric field coupling:

$$F_{E\text{-ph}} = -E_z(Z_P^* Q_P + Z_{A_{2u}}^* Q_{A_{2u}} + Z_{A_{1g}} Q_P Q_{A_{1g}}) - \sum_{j=x,y} E_j(Z_{E_u}^* Q_{E_u,j} + Z_{E_g} Q_P Q_{E_g,j}), \quad (4)$$

where $Z_{P,\text{IR}}^*$ are Born effective charges of the corresponding modes $Q_{P,\text{IR}}$, Z_{A_{1g},E_g} are coupling constants, $E_{x,y,z}$ are the electric field components.

It follows from Eq. (4) that coupling of the electric field to the centrosymmetric phonon modes A_{1g} and E_g is possible only in the ferroelectric phase, when $\langle Q_P \rangle \neq 0$. However, even in the ferroelectric phase this coupling is expected not to be large due to the small value of $\langle Q_P \rangle$. Indeed, the effective charge of $A_1(\text{TO}_3)$, which has irreducible representation A_{1g} in the paraelectric phase, is very small [30].

I will focus on a single phonon mode excitation and as a consequence only on two-phonon modes coupling, consisting of the ferroelectric soft mode Q_P and the infrared-active mode Q_{IR} (see Refs. [33,34] for discussions on three phonon modes interaction). The leading coupling terms in phonon amplitudes (up to the fourth order) are

$$F_{\text{ph-ph}} = \sum_{i=1,2} a_i Q_P^2 Q_{A_{1g}}^i + \sum_{i=1,2,3} c_i Q_P^i Q_{A_{2u}}^{4-i} + \sum_{\substack{i=g,u \\ j=x,y}} b_i Q_P^2 Q_{E_i,j}^2 + d Q_P Q_{E_u,y} (3Q_{E_u,x}^2 - Q_{E_u,y}^2). \quad (5)$$

Three-phonon interaction in Eq. (5) with the coupling constant a_1 is not of much interest because it is difficult to excite the A_{1g} mode as discussed above (since its effective charge is proportional to Q_P , this term is effectively of the fourth order in phonon coordinates).

The reversal of polarization by an electric field in LNO was discussed in detail in [35] and includes the nucleation of a domain (primarily at surface defects) and its forward and

sideways growth. These processes could be affected by crystal defects. This can explain the difference in the experimental values for the coercive field in the stoichiometric and congruent LNO equal to 40 and 210 kV/cm, respectively [36]. At the same time, the coercive field value, which follows from the phenomenological theory without defects, is about 5.4 MV/cm [37]. In my simplified theoretical model and calculations I consider a uniform polarization reversal and neglect the defects. I think that in the subpicosecond time scale of the experiment [19] along with the slow motion of the domain walls [35] my approach is justified.

Next, I apply the thermodynamic potential, Eq. (2), and the equation of motion, Eq. (1), to describe the results of the experiment [19] where the $A_1(\text{TO}_4)$ mode was pumped resonantly by a high-intensity femtosecond electromagnetic pulse. To do this, in the next section, I specify the numerical values of parameters that enter Eqs. (1) and (2).

IV. PARAMETER VALUES

The electric field in Eq. (4) has two components, $E_z = E_1 + E_2$, both directed along the z -axis in the experiment [19]. The first component is the electric field of the mid-infrared driving pulse $E_1(t) = E_0 \sin(\omega t) \exp(-4 \ln 2 t^2/T^2)$ with frequency ω , Gaussian envelope of duration $T = 0.15$ ps and amplitude E_0 , which is up to 25 MV/cm in the experiment [19], see Fig. 1(b). The other component is due to the depolarizing electric field E_d in the reverse polarization domain created by the midinfrared pump [Fig. 1(a)]. I suppose that on the time scale of the polarization reversal, as in the experiment [19], there is no screening of this field by free carriers. So, the resulting field is $E_2(t) = E_d(1 - Q_P(t)/Q_P^e)$.

I calculate the effective electric charges of infrared-active modes from the experimental values of their oscillation strength [38]. Thus I obtain $Z_P^* = 1.356$, $Z_{A_1(\text{TO}_2)}^* = 0.564$ and $Z_{A_1(\text{TO}_4)}^* = 1.404 e/\sqrt{u}$, where u is the atomic mass unit. The effective charge $Z_{A_1(\text{TO}_3)}^*$ is very small [31] and I will neglect the dynamics of this mode.

The value of Q_P^e , which is the initial value of Q_P in Eq. (1), can be determined from the change in ion positions at the ferroelectric phase transition. It is about $2.9\sqrt{u}$ Å, according to [4], which agrees with the minimum positions of the two-minimum energy surface calculated in [32]. At the same time, according to the experimental data [39], the Li and O atoms are shifted in the ferroelectric phase by about $\Delta z_{\text{Li}} = 0.460$ Å and $\Delta z_{\text{O}} = 0.270$ Å that gives $Q_P^e = (\sum_i m_i \Delta z_i^2)^{1/2} = 3.1\sqrt{u}$ Å. The same value of Q_P^e , which I adopt in my calculations, follows from the atomic displacements calculated *ab initio* [20–22]. Initial values of other coordinates are obtained from the equilibrium condition $\partial F/\partial Q_{\text{IR}} = 0$. They are not zero when the modes are nonlinearly coupled, see Fig. 1(b). This also can explain a partial overlap of ferroelectric soft modes in the para- and ferroelectric phases as discussed above.

I note that spontaneous polarization, defined as $P_s = Z_P^* Q_P^e/v_0$, with v_0 being the unit cell volume, is about 0.64 C/m² when calculating with $Q_P^e = 3.1\sqrt{u}$ Å. This is slightly lower than the experimental value for congruent crystals $P_s = 0.71$ C/m² [40,41], which, in turn, is achieved for a rather large value of $Q_P^e = 3.4\sqrt{u}$ Å. This slight discrepancy can

also be explained by the highly nonlinear evolution of the charges along the ferroelectric path of atomic displacements, which has a contribution from all infrared modes [21]. Note that even greater polarization of 0.82 [42] and 0.86 C/m² [43] was obtained by calculating *ab initio* surface charges, while the experimental value in a near-stoichiometric crystal is 0.62 ± 0.04 C/m² [44].

I take the damping constants at room temperature as $\tilde{\gamma}_P = 0.8$, $\tilde{\gamma}_{A_1(\text{TO}_2)} = 0.6$ and $\tilde{\gamma}_{A_1(\text{TO}_4)} = 1.0$ THz [38] (with $\gamma = 2\pi\tilde{\gamma}$). The damping $\tilde{\gamma}_P$ increases strongly with temperature and equals the soft mode frequency of 5 THz at about 1100 K [31]. As it was discussed in Sec. II, this would correspond to the transition from vibrational to relaxation mode dynamics in Eq. (1). Indeed, some experimental data, e.g., Ref. [39] and references therein, and molecular-dynamics simulations [45,46] suggest the transition from displacive to the order-disorder type phase transition in LNO near the critical temperature. This could imply that the damping $\tilde{\gamma}_P$ should depend on Q_P in Eq. (1). However, I note that the dynamics of Q_P is very fast in the experiment [19] and low-energy acoustic phonons, whose interaction time can not be shorter than the period of their oscillations, do not have time to exchange energy with Q_P and increase its damping. Thus I keep the damping $\tilde{\gamma}_P$ constant in my calculations.

Finally, I note that the biquadratic phonon-phonon interaction with the coupling constant c_2 in Eq. (5) does change not only the frequency of the soft mode Q_P but the frequency of the Q_{IR} as well, Eq. (3). This allows, for example, in some cases to reproduce the temperature dependence of polarization from the temperature dependence of frequency for high-frequency modes [47,48]. Usually the effect is not large. For the ferroelectric KH₂PO₄ crystal, however, the change is about ten percent for certain modes indicating both signs of the coupling constant [49,50]. So I calculate the coupling constant as $c_2 = (\omega_{\text{IR}}^2 - \Omega_{\text{IR}}^2)/2(Q_P^e)^2$ where ω_{IR} and Ω_{IR} are the frequencies of the Q_{IR} mode in the ferroelectric and paraelectric phases respectively, Q_P^e is the thermal equilibrium value of Q_P at room temperature. The positive sign of the coupling constant assures a single well potential $F(Q_P)$ for large values of Q_{IR}^2 and thus a possibility of the polarization reversal. I note that ω_{IR} does not change substantially in the ferroelectric phase of LNO up to about 1000 K [31,51], but this agrees with a small change in the polarization itself in this temperature range [52].

Due to the very high temperature of the phase transition, the values of Ω_{IR} in LNO are available only from the first-principles calculations. Being smaller than ω_{IR} , for $A_1(\text{TO}_4)$ they vary from 15.6 [20] and 14.3 [21] to 13.6 THz [22], while for $A_1(\text{TO}_2)$ from 3.5 [20] and 2.8 [21] down to 0.9 THz [22]. For $A_1(\text{TO}_3)$, on the contrary, the frequency in the paraelectric phase is higher, varying from 12.1 [20,21] to 10 THz [22], which indicates a possible negative value of the biquadratic phonon-phonon coupling constant for this mode. In my calculations, I take $\Omega_{A_1(\text{TO}_4)} = 14$ THz and $\Omega_{A_1(\text{TO}_2)} = 3.5$ THz, which correspond to $c_{2,A_1(\text{TO}_4)} = 34$ meV/u² Å⁴ and $c_{2,A_1(\text{TO}_2)} = 11$ meV/u² Å⁴. Note that these coupling constants are an order of magnitude smaller than those obtained for quantum paraelectric crystals KTaO₃ [53] and SrTiO₃ [54] from *ab initio* calculations. This might be due to the calculation procedure of the potential discussed in Sec. II.

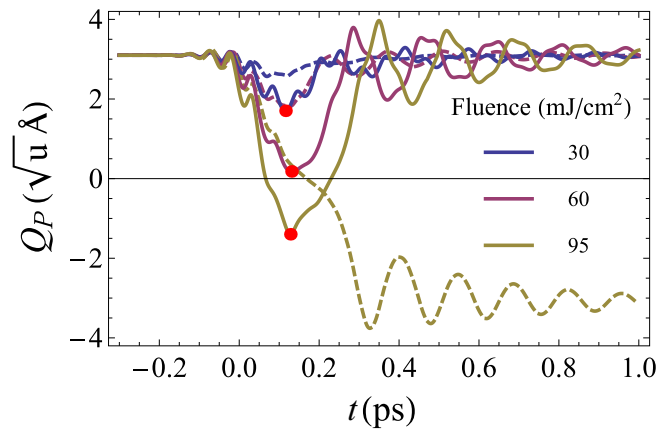


FIG. 2. Ferroelectric mode dynamics for the pump pulse fluences of 30, 60, and 95 mJ/cm² and frequency $\omega = 19$ THz when $c_{1,3} = 0$ and $E_d = 0$ (dashed) and $c_1 = 10$, $c_3 = 17$ meV/u² Å⁴ for $A_1(\text{TO}_4)$ and $E_d = 2.8$ MV/cm (solid). Red dots are at minimums of Q_P .

Indeed, if the crystal is not relaxed for every Q_P , as in Ref. [17], its energy $F(Q_P, Q_{\text{IR}})$ is higher and corresponds to larger coupling constants.

I keep the coupling constants c_1 and c_3 in Eq. (5) and the depolarizing electric field E_d in Eq. (4) as fitting parameters in my calculations, which I compare to the experiment [19].

V. CALCULATION RESULTS

I start with zero values of the coupling constants $c_{1,3}$ and the depolarizing electric field E_d and calculate the phonon mode dynamics for several values of the pump pulse fluence, see Fig. 2. In the experiment [19], for fluences above the threshold value of 60 mJ/cm², the disappearance of the second-harmonic intensity (and hence the ferroelectric mode amplitude Q_P) was observed at some point. I see, however, only its decrease with this fluence. The dynamics becomes closer to the experiment [19] when $c_{2,A_1(\text{TO}_4)} = 51$ meV/u² Å⁴, which corresponds, however, to the very low frequency $\Omega_{A_1(\text{TO}_4)} = 10.7$ THz expected in the paraelectric phase. Interestingly, the situation can be improved when positive values of $c_{3,A_1(\text{TO}_4)} \gtrsim 13$ meV/u² Å⁴ are considered. This is rather unexpected, because the force arising from this coupling and acting on Q_P oscillates and changes its sign. At the same time, negative values of $c_{3,A_1(\text{TO}_4)}$ make the polarization reversal even harder. Finite values of $c_{1,A_1(\text{TO}_4)}$ do not influence much the dynamics. The reason is that the latter coupling is cubic in Q_{IR} , while the former is linear and $Q_{\text{IR}} \ll Q_P$.

The reentrant behavior of the polarization for the highest fluence of 95 mJ/cm² available in Ref. [19] appears for depolarizing electric fields greater than about $E_d \approx 2.5$ MV/cm. This value to be compared with the depolarizing field in a platelike monodomain sample $E_d = P_s/(\epsilon\epsilon_0)$, which is about 26.4 MV/cm for $P_s = 0.70$ C/m² and the dielectric constant $\epsilon_{33} = 30$ in LNO [37,55] (ϵ_0 is the electric constant). The value of the depolarization factor $N \approx 0.1$ seems reasonable given the oblong shape of the created domain with reverse polarization (the pump penetration depth is about 3.2 μm [19] and its spot size is about 65 μm [38], see Fig. 1(a)).

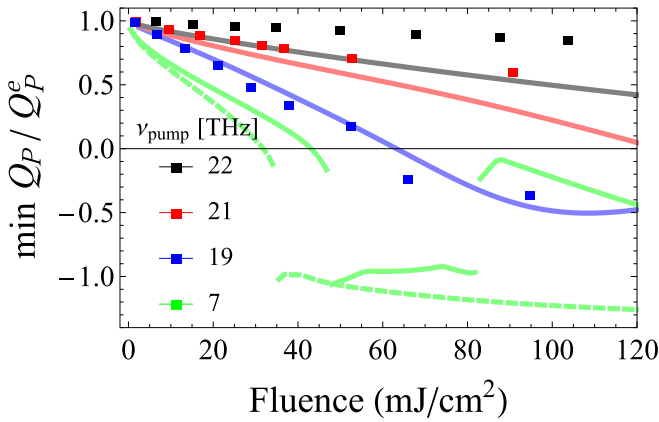


FIG. 3. Minimum of Q_P (normalized by Q_P^e) as a function of fluence for different frequencies of the pump pulse. At $\nu_{\text{pump}} = 7$ THz two lines correspond to opposite signs of the pump pulse electric field. Experimental data points are from Ref. [19].

Finally, I use the values $E_d = 2.8$ MV/cm and $c_1 = 10$ and $c_3 = 17$ meV/u² Å⁴ for the mode $A_1(\text{TO}_4)$, see Fig. 2. I keep the coupling constants $c_{1,3}$ equal to zero for the mode $A_1(\text{TO}_2)$, which is close in frequency to Q_P , since its effect on the dynamics of the latter is in any case masked by the direct excitation of Q_P .

I calculate the minimum value of Q_P (normalized by Q_P^e) as a function of fluence for different frequencies of the pump pulse (with the same Gaussian envelope duration) and compare the results to the experiment [19], see Fig. 3. The agreement is very good for the pump frequency of 19 THz. For other frequencies, the dependence on fluence is also close to linear, but the coefficient is somewhat different from the experiment [19]. This can be due to the differences in the infrared phonon damping constant and the pump pulse duration, which determines its frequency width, in my calculations compared to the experiment [19].

For a pump frequency of 7 THz close to the ferroelectric mode resonance, the result depends slightly on the sign (phase) of the pulse oscillations due to comparable values of the pump duration and its oscillation period. For this pump frequency, a final change in polarization is observed for fluences exceeding approximately 40 mJ/cm². Reversing the polarization becomes more difficult if a larger value of the depolarizing field is assumed until it becomes impossible if $E_d \gtrsim 5$ MV/cm. This threshold corresponds to the value of the coercive field in my model, $E_c = P_s/(3\sqrt{3}\epsilon\epsilon_0)$, at which the metastable state (local minimum) with opposite polarization disappears [37].

The susceptibility, $\min Q_P/\text{fluence}$, calculated for small fluences as a function of the pump frequency also reproduces the experimental results [19] (Fig. 4). The width of the peaks is determined mainly by the frequency width of the pump pulse.

VI. DISCUSSION

In my calculations, oscillations of Q_P with the frequency of the ferroelectric mode are observed, Fig. 2. In the experiment [19], these oscillations could be smeared out for several

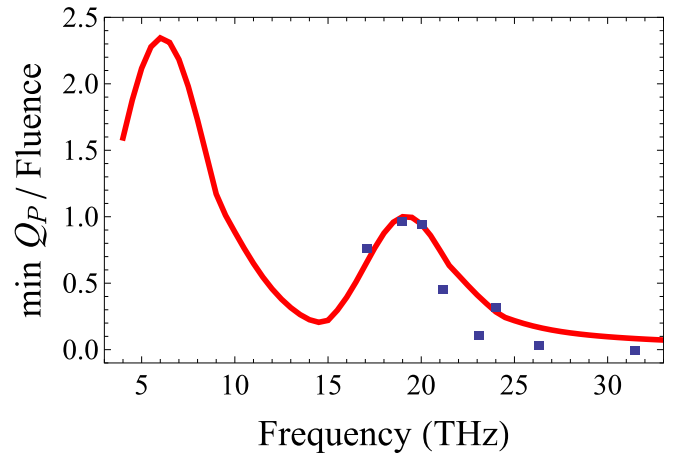


FIG. 4. Susceptibility as a function of the pump frequency normalized to unity at 19 THz. Experimental data points are from Ref. [19].

reasons. First, the electric field of the midinfrared pulse is inhomogeneous in the crystal and is determined by the Gaussian function perpendicular to its direction and exponentially drops from the surface as $\exp(-z/z_0)$ with $z_0 \approx 3.5$ μm, while the second harmonic is generated at $z \lesssim 1$ μm [19]. Second, the nonlinear coupling to phonon modes with nonzero wave numbers, which I did not take into account, will probably also lead to some smearing of polarization oscillations. Finally, I have neglected fluctuations in Eq. (1), as it was discussed in Sec. II. For a harmonic oscillator with a frequency ω , these fluctuations are equal to $\langle \delta Q^2 \rangle = (\hbar/\omega)(1/2 + (e^{\hbar\omega/T} - 1)^{-1})$ [23,26], in accordance with the fluctuation-dissipation theorem [23]. At zero temperature, this gives $\langle \delta Q_{\text{IR}}^2 \rangle = 0.17$ and $\langle \delta Q_P^2 \rangle = 0.26 \sqrt{u}$ Å, which are an order of magnitude smaller than the amplitudes of these coordinates around 2 and 3.1 \sqrt{u} Å (see Figs. 1 and 2), in reasonable agreement with the approximation used. At room temperature, the fluctuations become twice as large for the ferroelectric mode, but still small enough, and little change for the high-frequency infrared mode. I note that these fluctuations relate to phonon coordinates and, through Eq. (1), affect their averages defining polarization. At the same time, the relative fluctuation for macroscopic polarization, defined as a dipole per unit volume, is inversely proportional to the square root of the number of dipoles per unit volume and is therefore extremely small.

Recently, high-intensity sources of far-infrared electromagnetic fields (more than 3.5 MV/cm), tunable in the range from 4 to 18 THz, were reported in Ref. [56]. These fluences, however, are not high enough to switch polarization by resonant pumping of the ferroelectric mode (Fig. 3). In Ref. [57], a very high-intensity source of a terahertz single-cycle pulse (up to 22 MV/cm) was reported, but its frequency is only about 1 THz. Thus the resonant reversal of the ferroelectric mode in LNO currently seems unattainable.

My calculations show that the polarization can eventually be switched in the absence of a depolarizing field (Fig. 2). To screen this field, one can use a metallic wire drawn in gold in Fig. 5. The relaxation time of this screen $\tau = RC$ is determined by the resistance $R \approx \rho L/(h+d)\delta$ and the capacitance $C \approx \epsilon\epsilon_0 h$ of the wire. The resistivity and skin

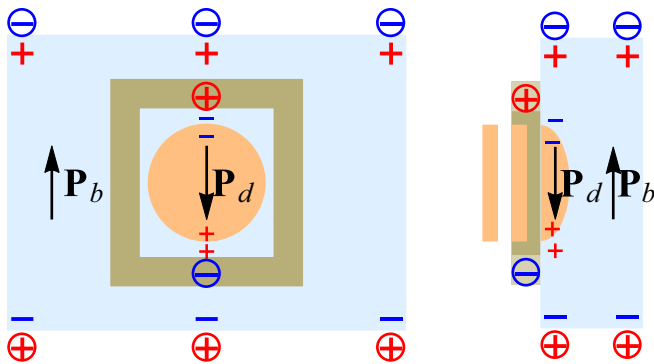


FIG. 5. Sketch of the screen (in golden) on the top of the crystal around the pump laser spot and the electric charges distribution (free charges are in circles).

depth for gold at frequency 10 THz are $\rho \sim 10^{-7} \Omega \text{ m}$ and $\delta \approx 30 \text{ nm}$. The metallic wire length, height and width are about $L \approx 400 \mu\text{m}$, $h \sim d \sim 10\text{--}100 \mu\text{m}$. This yields a relaxation time less than $\tau \sim 0.1 \text{ ps}$, which is enough to follow the polarization dynamics (Fig. 2).

Anharmonic oscillations of the lowest frequency E mode in LNO under resonant excitation by a single-cycle pulse with the electric field of about 1 MV/cm have recently been investigated [58]. At the same time, it would be interesting to see the dynamics of the ferroelectric mode Q_P induced by the resonant excitation of E modes, Eqs. (4) and (5), especially given the orthogonal polarizations of the A and E

modes. The calculated *ab initio* frequencies of the E modes in LNO [20,22] differ significantly in the para- and ferroelectric phases, indicating possible strong coupling constants of these modes with the ferroelectric mode.

VII. CONCLUSIONS

The calculations of the ferroelectric mode dynamics in LNO, determined by the parent phase symmetry-invariant thermodynamic potential, well reproduce the transient reversal of polarization under the high-frequency mode excitation [19] when the electric field of bound charges is taken into account. The estimated strength of this field is consistent with the polarization value in LNO and the expected depolarization factor of the transiently created polarization domain. I argue that the polarization can eventually be reversed if the depolarizing field is screened, for example, by a metallic wire on top of the crystal around the pump laser spot. I predict that similar polarization dynamics in LNO can be obtained by resonant excitation of the E modes orthogonal to spontaneous polarization. A good indicator of other materials with strong nonlinear phonon couplings to the ferroelectric mode can be the change in the frequency of infrared phonons during the ferroelectric phase transition.

ACKNOWLEDGMENTS

I thank R. Mankowsky and A. Subedi for useful discussions. The study was carried out with the financial support of the Russian Foundation for Basic Research in the framework of the scientific Project No. 18-02-00399.

- [1] J. F. Scott, Applications of modern ferroelectrics, *Science* **315**, 954 (2007).
- [2] A. Kakekhani, S. Ismail-Beigi, and E. I. Altman, Ferroelectrics: A pathway to switchable surface chemistry and catalysis, *Surf. Sci.* **650**, 302 (2016).
- [3] S. Sanna and W. G. Schmidt, LiNbO₃ surfaces from a microscopic perspective, *J. Phys.: Condens. Matter* **29**, 413001 (2017).
- [4] M. Lines and A. Glass, *Principles and Applications of Ferroelectrics and Related Materials*, International Series of Monographs on Physics (OUP, Oxford, 2001).
- [5] Y. Xu, *Ferroelectric Materials and their Applications* (Elsevier, Amsterdam, Netherlands, 1991).
- [6] J. Li, B. Nagaraj, H. Liang, W. Cao, C. H. Lee, and R. Ramesh, Ultrafast polarization switching in thin-film ferroelectrics, *Appl. Phys. Lett.* **84**, 1174 (2004).
- [7] S. Fahy and R. Merlin, Reversal of Ferroelectric Domains by Ultrashort Optical Pulses, *Phys. Rev. Lett.* **73**, 1122 (1994).
- [8] T. Qi, Y.-H. Shin, K.-L. Yeh, K. A. Nelson, and A. M. Rappe, Collective Coherent Control: Synchronization of Polarization in Ferroelectric PbTiO₃ by Shaped THz Fields, *Phys. Rev. Lett.* **102**, 247603 (2009).
- [9] R. Herchig, C.-M. Chang, B. K. Mani, and I. Ponomareva, An unusual route to polarization reversal in ferroelectric ultrathin nanowires, *Appl. Phys. Lett.* **105**, 012907 (2014).
- [10] C. Lian, Z. A. Ali, H. Kwon, and B. M. Wong, Indirect but efficient: Laser-excited electrons can drive ultrafast polarization switching in ferroelectric materials, *J. Phys. Chem. Lett.* **10**, 3402 (2019).
- [11] Y. Okimoto, S. Naruse, R. Fukaya, T. Ishikawa, S. Koshihara, K. Oka, M. Azuma, K. Tanaka, and H. Hirori, Ultrafast Control of the Polarity of BiCoO₃ by Orbital Excitation as Investigated by Femtosecond Spectroscopy, *Phys. Rev. Appl.* **7**, 064016 (2017).
- [12] Y.-H. Kuo, S. Nah, K. He, T. Hu, and A. M. Lindenberg, Ultrafast light-induced symmetry changes in single BaTiO₃ nanowires, *J. Mater. Chem. C* **5**, 1522 (2017).
- [13] K. A. Brekhov, K. A. Grishunin, D. V. Afanas'ev, S. V. Semin, N. E. Sherstyuk, E. D. Mishina, and A. V. Kimel, Optical second harmonic generation and its photoinduced dynamics in ferroelectric semiconductor Sn₂P₂S₆, *Phys. Solid State* **60**, 31 (2018).
- [14] K. A. Grishunin, N. A. Ilyin, N. E. Sherstyuk, E. D. Mishina, A. Kimel, V. M. Mukhortov, A. V. Ovchinnikov, O. V. Chefonov, and M. B. Agranat, THz electric field-induced second harmonic generation in inorganic ferroelectric, *Sci. Rep.* **7**, 687 (2017).
- [15] E. Mishina, K. Grishunin, V. Bilyk, N. Sherstyuk, A. Sigov, V. Mukhortov, A. Ovchinnikov, and A. Kimel, Polarization switching in ferroelectric thin film induced by a single-period terahertz pulse, *MRS Adv.* **3**, 1901 (2018).
- [16] A. Stupakiewicz, K. Szerenos, D. Afanasiev, A. Kirilyuk, and A. V. Kimel, Ultrafast nonthermal photo-magnetic recording in a transparent medium, *Nature (London)* **542**, 71 (2017).
- [17] A. Subedi, Proposal for ultrafast switching of ferroelectrics using midinfrared pulses, *Phys. Rev. B* **92**, 214303 (2015).

- [18] M. Först, C. Manzoni, S. Kaiser, Y. Tomioka, Y. Tokura, R. Merlin, and A. Cavalleri, Nonlinear phononics as an ultrafast route to lattice control, *Nat. Phys.* **7**, 854 (2011).
- [19] R. Mankowsky, A. von Hoegen, M. Först, and A. Cavalleri, Ultrafast Reversal of the Ferroelectric Polarization, *Phys. Rev. Lett.* **118**, 197601 (2017).
- [20] K. Parlinski, Z. Q. Li, and Y. Kawazoe, *Ab initio* calculations of phonons in LiNbO₃, *Phys. Rev. B* **61**, 272 (2000).
- [21] M. Veithen and P. Ghosez, First-principles study of the dielectric and dynamical properties of lithium niobate, *Phys. Rev. B* **65**, 214302 (2002).
- [22] M. Friedrich, A. Riefer, S. Sanna, W. G. Schmidt, and A. Schindlmayr, Phonon dispersion and zero-point renormalization of LiNbO₃ from density-functional perturbation theory, *J. Phys.: Condens. Matter* **27**, 385402 (2015).
- [23] L. Landau and E. Lifshitz, *Statistical Physics*, Course of Theoretical Physics, Vol. 5 (Elsevier Science, Amsterdam, Netherlands, 2013).
- [24] V. Ginzburg, A. Levanyuk, and A. Sobyenin, Light scattering near phase transition points in solids, *Phys. Rep.* **57**, 151 (1980).
- [25] L. Landau and E. Lifshitz, *Quantum Mechanics: Non-Relativistic Theory*, Course of Theoretical Physics, Vol. 3 (Elsevier Science, Amsterdam, Netherlands, 1981).
- [26] A. Messiah, *Quantum Mechanics*, Dover Books on Physics (Dover, Mineola, NY, 1999).
- [27] R. Blinc and B. Žekš, *Soft Modes in Ferroelectrics and Antiferroelectrics*, Selected Topics in Solid State Physics (North-Holland, Amsterdam, Netherlands, 1974).
- [28] S. Margueron, A. Bartaszyte, A. M. Glazer, E. Simon, J. Hlinka, I. Gregora, and J. Gleize, Resolved E-symmetry zone-centre phonons in LiTaO₃ and LiNbO₃, *J. Appl. Phys.* **111**, 104105 (2012).
- [29] S. Sanna, S. Neufeld, M. Rüsing, G. Berth, A. Zrenner, and W. G. Schmidt, Raman scattering efficiency in LiTaO₃ and LiNbO₃ crystals, *Phys. Rev. B* **91**, 224302 (2015).
- [30] S. Kojima, K. Kanehara, T. Hoshina, and T. Tsurumi, Optical phonons and polariton dispersions of congruent LiNbO₃ studied by far-infrared spectroscopic ellipsometry and Raman scattering, *Jpn. J. Appl. Phys.* **55**, 10TC02 (2016).
- [31] A. Ridah, M. D. Fontana, and P. Bourson, Temperature dependence of the Raman modes in LiNbO₃ and mechanism of the phase transition, *Phys. Rev. B* **56**, 5967 (1997).
- [32] I. Inbar and R. E. Cohen, Origin of ferroelectricity in LiTaO₃ and LiNbO₃ LAPW total energy calculations, *Ferroelectrics* **164**, 45 (1995).
- [33] D. M. Juraschek, M. Fechner, and N. A. Spaldin, Ultrafast Structure Switching through Nonlinear Phononics, *Phys. Rev. Lett.* **118**, 054101 (2017).
- [34] P. G. Radaelli, Breaking symmetry with light: Ultrafast ferroelectricity and magnetism from three-phonon coupling, *Phys. Rev. B* **97**, 085145 (2018).
- [35] V. Y. Shur, Kinetics of ferroelectric domains: Application of general approach to LiNbO₃ and LiTaO₃, *J. Mater. Sci.* **41**, 199 (2006).
- [36] S. Kim, V. Gopalan, and A. Gruverman, Coercive fields in ferroelectrics: A case study in lithium niobate and lithium tantalate, *Appl. Phys. Lett.* **80**, 2740 (2002).
- [37] T. Volk and M. Wöhlecke, *Lithium Niobate* (Springer Berlin Heidelberg, 2008).
- [38] A. von Hoegen, R. Mankowsky, M. Fechner, M. Först, and A. Cavalleri, Probing the interatomic potential of solids with strong-field nonlinear phononics, *Nature (London)* **555**, 79 (2018).
- [39] H. Boysen and F. Altorfer, A neutron powder investigation of the high-temperature structure and phase transition in LiNbO₃, *Acta Crystallogr., Sect. B* **50**, 405 (1994).
- [40] S. H. Wemple, M. DiDomenico, and I. Camlibel, Relationship between linear and quadratic electro-optic coefficients in LiNbO₃, LiTaO₃, and other oxygen-octahedra ferroelectrics based on direct measurement of spontaneous polarization, *Appl. Phys. Lett.* **12**, 209 (1968).
- [41] F. Johann and E. Soergel, Quantitative measurement of the surface charge density, *Appl. Phys. Lett.* **95**, 232906 (2009).
- [42] S. Sanna, R. Hölscher, and W. Schmidt, Temperature dependent LiNbO₃(0001): Surface reconstruction and surface charge, *Appl. Surf. Sci.* **301**, 70 (2014).
- [43] S. V. Levchenko and A. M. Rappe, Influence of Ferroelectric Polarization on the Equilibrium Stoichiometry of Lithium Niobate (0001) Surfaces, *Phys. Rev. Lett.* **100**, 256101 (2008).
- [44] Y.-L. Chen, J.-J. Xu, X.-J. Chen, Y.-F. Kong, and G.-Y. Zhang, Domain reversion process in near-stoichiometric LiNbO₃ crystals, *Opt. Commun.* **188**, 359 (2001).
- [45] S. R. Phillpot and V. Gopalan, Coupled displacive and order-disorder dynamics in LiNbO₃ by molecular-dynamics simulation, *Appl. Phys. Lett.* **84**, 1916 (2004).
- [46] S. Sanna and W. G. Schmidt, Ferroelectric phase transition in LiNbO₃: Insights from molecular dynamics, *IEEE Trans. Ultrason., Ferroelectrics Frequency Control* **59**, 1925 (2012).
- [47] A. S. Krylov, A. N. Vtyurin, A. S. Oreshonkov, V. N. Voronov, and S. N. Krylova, Structural transformations in a single-crystal Rb₂NaYF₆: Raman scattering study, *J. Raman Spectrosc.* **44**, 763 (2013).
- [48] E. K. H. Salje and U. Bismayer, Hard mode spectroscopy: The concept and applications, *Phase Transitions* **63**, 1 (1997).
- [49] F. Brehat and B. Wyncke, Low-frequency models in KH₂PO₄-type crystals, *Int. J. Infrared Millimeter Waves* **8**, 155 (1987).
- [50] P. Simon, F. Gervais, and E. Courtens, Paraelectric-ferroelectric phase transitions of KH₂PO₄, RbH₂PO₄, and KH₂AsO₄ studied by infrared reflectivity, *Phys. Rev. B* **37**, 1969 (1988).
- [51] W. D. Johnston and I. P. Kaminow, Temperature dependence of raman and rayleigh scattering in LiNbO₃ and LiTaO₃, *Phys. Rev.* **168**, 1045 (1968).
- [52] R. I. Shostak, S. V. Yevdokimov, and A. V. Yatsenko, An analysis of the temperature dependence of the spontaneous polarization of LiNbO₃ crystals, *Crystallogr. Rep.* **54**, 492 (2009).
- [53] A. Subedi, Midinfrared-light-induced ferroelectricity in oxide paraelectrics via nonlinear phononics, *Phys. Rev. B* **95**, 134113 (2017).
- [54] M. Kozina, M. Fechner, P. Marsik, T. van Driel, J. M. Glownia, C. Bernhard, M. Radovic, D. Zhu, S. Bonetti, U. Staub, and M. C. Hoffmann, Terahertz-driven phonon upconversion in SrTiO₃, *Nat. Phys.* **15**, 387 (2019).
- [55] R. S. Weis and T. K. Gaylord, Lithium niobate: Summary of physical properties and crystal structure, *Appl. Phys. A* **37**, 191 (1985).

- [56] B. Liu, H. Bromberger, A. Cartella, T. Gebert, M. Först, and A. Cavalleri, Generation of narrowband, high-intensity, carrier-envelope phase-stable pulses tunable between 4 and 18THz, *Opt. Lett.* **42**, 129 (2017).
- [57] A. V. Ovchinnikov, O. V. Chefonov, E. D. Mishina, and M. B. Agranat, Second harmonic generation in the bulk of silicon induced by an electric field of a high power terahertz pulse, *Sci. Rep.* **9**, 9753 (2019).
- [58] B. S. Dastrup, J. R. Hall, and J. A. Johnson, Experimental determination of the interatomic potential in LiNbO_3 via ultrafast lattice control, *Appl. Phys. Lett.* **110**, 162901 (2017).